

Vertical midscale ionospheric disturbances caused by surface seismic waves based on Irkutsk chirp ionosonde data in 2011-2016.

O.I. Berngardt, N.P. Perevalova, A.V. Podlesnyi, V.I. Kurkin, G.A. Zhrebtsov

January 29, 2022

Abstract

Based on the Irkutsk fast monostatic chirp ionosonde data we made a statistical analysis of ionospheric effects for 28 earthquakes which appeared in 2011-2016 years. These effects are related with surface (Rayleigh) seismic waves far from epicenter. The analysis has shown that nine of these earthquakes were accompanied by vertical midscale ionospheric irregularities (multicusp). To estimate the ionospheric efficiency of the seismic waves we proposed new index K_W . The index estimates the maximal amplitude of the acoustic shock wave generated by given spatial distribution of seismic vibrations and related with maximal spectral power of seismic oscillations.

Based on the analysis of experimental data we have shown that earthquake-related multicusp is observed mostly at daytime [07:00-17:00]LST for $K_W \geq 4.7$. The observations of intrinsic gravity waves by GPS technique in the epicenter vicinity do not show such a daytime dependence. Based on 24/05/2013 Okhotsk Sea earthquake example, we demonstrated that deep-focus earthquakes can produce strong multicusp far from the epicenter, although do not produce significant GPS ionospheric response in the epicenter vicinity. Three cases of sporadic E bifurcation in far epicentral zone were also detected and discussed.

1 Introduction

The investigation of ionospheric effects caused by the Earth's surface sources is a traditional and effective technique for studies of neutral-ionospheric interaction. A lot of papers are devoted to theoretical and experimental

aspects of the problem [Blanc (1985), Pokhotelov (1995), Lognonné et al. (1998), Laštovička (2006), Kiryushkin et al. (2011), Jin et al. (2015)].

One of such phenomena is generation of midscale ionospheric irregularities directly by shock wave from the supersonic seismic source propagating over the surface [Maruyama et al. (2011), Liu et al. (2011), Rolland (2011), Kakinami et al. (2013), Maruyama and Shinagawa (2014), Bergardt et al. (2015), Maruyama et al. (2016a), Maruyama et al. (2016b), Kherani et al. (2016), Chum et al. (2016), Liu et al. (2016)].

To estimate the seismic disturbance efficiency to the ionosphere is the essential problem for planning and interpretation of each single experiment. The effective generation of intrinsic gravity waves (IGW) in the vicinity of the epicenter according to GPS-data requires large enough earthquake magnitude [Perevalova et al. (2014)]. But there are no statistical information about the boundary values for the intensity of seismic (Rayleigh) waves that produce the vertical midscale ionospheric structures (multicusp).

For the study of the multicusp the vertical ionosondes are widely used [Maruyama et al. (2011), Maruyama and Shinagawa (2014), Maruyama et al. (2016a), Maruyama et al. (2016b)]. The use of chirp ionosondes for this problem significantly increases the signal-to-noise ratio and improves the temporal and spatial resolution, which are the key parameters for such studies. The efficiency of replacement of the pulse ionosondes by chirp ionosondes for diagnosis of ionospheric profile was demonstrated, for example in [Harris et al. (2016)].

Baikal region is a seismically active area, so studies of seismic activity effects are constantly being conducted. A number of various ionospheric, optical, magnetic, seismic and acoustic instruments are involved into monitoring and case-study tasks [Zherebtsov et al. (2012)].

The aim of this paper is a preliminary statistical analysis of the emergence of midscale vertical ionospheric irregularities caused by large earthquakes at a large distance from the epicenter and investigating the effectiveness of this mechanism. In order to complete this, we used the 2011-2016 data from the Irkutsk fast monostatic chirp ionosonde (IFMCI). We also used a variety of GPS-receivers in the areas near the epicenters of the earthquakes to compare near zone and far zone ionospheric effects.

2 Data used in the experiments

2.1 Chirp ionosonde

IFMCI (51.81N, 103.078E) started its continuous operation in 2012, 150 km to the South-West from Irkutsk. For operation it uses a continuous chirp-signal with a frequency range from 1.5 MHz to 15 MHz and 10Watts

of transmitted power [Podlesnyi et al (2011), Podlesnyi et al (2013)]. The spacing between the receiving and transmitting antenna is approximately 150 meters. Low power and minimal spacing between antennas allows transmitter and receiver to operate at the same time.

The use of modern technologies of digital reception allows us to reach a high flexibility in the use of equipment and get a wide dynamic range. The fully digital structure of the ionosonde allows us to precisely control the shape of the transmitted signal as well as the impulse response and filtering characteristics of the receivers [Podlesnyi et al (2011)]. We develop and use original techniques for filtering out the signals from neighbor public radiostations and significantly improve the quality of the ionosonde data [Podlesnyi et al (2014a)].

The typical frequency sweep speed is about 500 kHz/s, providing 27 second time resolution. From the beginning of its continuous operation in 2012 the ionosonde uses 1-minute time resolution typical for modern monitoring techniques [Reinisch et al (2009), Akchurin et al. (2011), Harris et al. (2012), Kurkin et al. (2014)]. This allows us to use its data for detailed study of vertical ionospheric disturbances generated by seismic waves.

2.2 Seismic data sources

For analysis of seismic variations we use the data from Talaya seismic station (TLY, 51.681N, 103.644E, [IRIS/IDA Seismic Network ()], Synthetic Seismograms Network ()). The station is located near the point of ionospheric sounding, and both of them are marked at Fig.1A by single vertical cross. For analysis of the results presented in other publications, we used the data from seismic stations ARU (56.429N, 58.561E, [IRIS/IDA Seismic Network ()]), NKC (50.233N, 12.448E, [Synthetic Seismograms Network ()]) and TATO (24.973N, 121.497E, [Global Seismograph Network ()]), also located near the points of corresponding ionospheric observations.

Strong earthquakes at large distances from the epicenter sometimes produce in the ionosphere vertical midscale irregularities (multicusp) [Maruyama et al. (2011)]. Their generation is associated with the passage of supersonic surface (Rayleigh) seismic waves below the point of ionospheric sounding [Rolland (2011), Maruyama et al. (2011), Liu et al. (2011), Chum et al. (2012), Kakinami et al. (2013), Maruyama and Shinagawa (2014), Bergardt et al. (2015), Maruyama et al. (2016a), Maruyama et al. (2016b), Liu et al. (2016)], and with propagation of resulting acoustic shock wave in the atmosphere and ionosphere.

The amplitude of the effect is determined by the amplitude of the source seismic vibrations. So selecting the earthquakes that produce the effect over their magnitude, the distance to them, or other parameters of the earthquake

related to epicenter is not optimal. To select the earthquakes participating in the study, we analyzed the amplitude of the seismic vibrations near the point of ionospheric observations. We estimated the equivalent class K_A of the earthquake seismic vibrations by representing the observed vertical seismic amplitude in logarithmic scale. This gives us a rough estimation of the amplitude of the source of the shock wave in the ionosphere at large distances from the epicenter. The K_A is:

$$K_A = 10 \cdot \max \{ \log_{10}(\tilde{h}) - 5 \}$$

where \tilde{h} is the amplitude of the vertical seismic oscillations (in nanometers), calculated as the median over 4 seconds to remove noise. Table1 shows the list of detected at TLY station large seismic disturbances with $K_A > 6$, that were analyzed in the paper, and corresponding earthquakes.

Fig. 1A shows the geometry of investigated earthquakes, marked by circles with radius proportional to their K_A , measured at TLY station. As one can see, the earthquakes at larger distances appear with a smaller K_A , than the earthquakes at smaller distances from seismic station. This illustrates the local character of the K_A class, related with not only the earthquake magnitude, but with the relative position of the epicenter and seismic station also.

2.3 GPS receivers network

Investigation of the ionospheric total electron content variations (TEC) in the vicinity of the earthquake epicenters was made on the basis of phase measurements at dual frequency GPS receivers. For every given earthquake epicenter the data from nearby GPS-stations from International hemodynamic network IGS (<http://sopac.ucsd.edu>) were used for this study.

TEC variations were calculated by the standard technique used to study the earthquake effects [Calais and Minster (1995), Afraimovich et al. (2001a), Astafyeva et al. (2009)]. In accordance with generally accepted standards, we relate the measured TEC with the ionospheric point, i.e. with the point of intersection of the ray "satellite-receiver" with equivalent ionospheric layer at the height of maximal electron density h_{max} [Calais and Minster (1995), Afraimovich et al. (2001a), Astafyeva et al. (2009), Astafyeva et al. (2013), Perevalova et al. (2014), Perevalova et al. (2015)]. In our research we used typical $h_{max} = 300km$. We filtered the initial TEC series to get the variations with periods ranging from 2 to 10 minutes, typically intensified by earthquakes in the vicinity of the epicenter [Calais and Minster (1995), Afraimovich et al. (2001a),

Astafyeva et al. (2009), Astafyeva et al. (2013), Perevalova et al. (2014)] and related with the midscale ionospheric disturbances caused by earthquakes.

To make more accurate comparison of the intensity of ionospheric disturbances at different stations we transform the inclined TEC variations into equivalent vertical TEC variations [Afraimovich et al. (2001a), Astafyeva et al. (2013), Perevalova et al. (2015)]. To differ earthquake effects from regular one we compared the TEC variations at the day of the earthquake with TEC variations in previous and subsequent days, following to traditional approach [Afraimovich et al. (2001a), Perevalova et al. (2014), Perevalova et al. (2015)].

3 Observations of vertical midscale ionospheric irregularities related with surface seismic waves far from epicenter

3.1 F-layer multicusp: ionogrames at the moment of disturbance

One of the effects observed after a powerful earthquake is 'multicusp' in the ionosphere, associated with the passage of powerful shock wave (Mach cone) from supersonic surface seismic waves (Rayleigh waves). The propagation of shock wave in the neutral atmosphere generates similar irregularities in the ionosphere through the neutral-ion collisions (see, for example [Maruyama and Shinagawa (2014)]). These ionospheric irregularities can be detected by vertical ionosondes, in a form of very specific, short-lived disturbances at the ionograms. This phenomenon was clearly observed after the Tohoku earthquake 11/03/2011 [Maruyama and Shinagawa (2014), Maruyama et al. (2011), Matsumura et al. (2011), Liu et al. (2013), Berngardt et al. (2015)] and after Chile earthquake 27/02/2010 [Maruyama et al. (2016b)]. Usually this effect is very fast: its total duration is associated with the passage of the surface seismic waves, and usually do not exceed several minutes. Therefore, for its diagnosis one needs the ionospheric instruments with temporal resolution better than 1 minute - a network of GPS-receivers or fast ionosondes. The weakness of the effect even after strong earthquakes makes possible their observation with GPS in either case of the most powerful earthquakes (when disturbances in the total electron content are significant), or with large spatial networks of GPS-receivers using special processing and accumulation techniques presented, for example, in [Afraimovich et al. (2000), Afraimovich et al. (2001b)].

In comparison with GPS-receiver, covering huge spatial area and allowing us to investigate mostly horizontal structure of the irregularities, the ionosonde

usually investigates ionosphere above its location. Ionosondes are more sensitive instruments for investigating the midscale vertical irregularities, and, thus, they are more useful than GPS for analysis of vertical ionospheric disturbances after weaker earthquakes or effects at larger distances from the epicenter.

The only drawback of ionosondes is their poor temporal resolution of the order of 10-15 minutes intended mainly for the diagnosis of secondary ionospheric parameters - the behavior of critical frequencies and the height of the maximum. Ionosondes with a higher temporal resolution were suggested and used for case studies a long time ago [Munro and Heisler (1956), Ponyatov et al. (1999)], but for regular studies they appeared quite recently [Reinisch et al (2009), Akchurin et al. (2011), Harris et al. (2012), Berngardt et al. (2015), Harris et al. (2016), Maruyama et al. (2016a), Maruyama et al. (2016b), Kozlovsky et al. (2013)]. IFMCI has the necessary temporal resolution [Berngardt et al. (2015)] and works in 1 minute mode constantly - since 2012, and selectively - since 2011. This allowed us to accumulate a huge statistics for monitoring of ionospheric perturbations associated with earthquakes in this period.

Fig.2 shows an example of the dynamics of vertical ionospheric disturbances ('multicusp') at Irkutsk ionosonde data during deep Okhotsk Sea earthquake (24/05/2013), rarely discussed in the literature. The most significant multicusp effect is observed up to 300km effective height during 06:02-06:06UT. As one can see, the effect duration is about several minutes. This makes it difficult for detection by standard 15-minute ionosondes. The effect is observed about 7-10 minutes after the moment of maximal seismic vertical variation. This delay is related with propagation of acoustic signal from the ground to these heights, and explains well experimental observations [Maruyama et al. (2011), Matsumura et al. (2011), Liu et al. (2013), Berngardt et al. (2015), Maruyama et al. (2016a), Maruyama et al. (2016b)].

To analyze seismic effects in the ionosphere we analyzed the ionograms in the period ± 15 minutes from the beginning(end) of most powerful seismic disturbances during the investigated period. The ionograms related to each seismic disturbance are shown in Support Materials. As a result, we found that the 'multicusp' effect of earthquakes at IFMCI data was observed during the following earthquakes: 11/03/2011 (Mw9.0 Tohoku, Japan), 26/02/2012 (Mw6.6 Southwestern Siberia, Russia), 11/04/2012 (Mw8.4 Northern Sumatra), 11/04/2012 (Mw8.0 Northern Sumatra), 24/05/2013 (Mw8.3 Okhotsk Sea), 26/04/2015 (Mw6.7 Nepal), 12/05/2015 (Mw7.3 Nepal), 17/09/2015 (Mw8.3 Coquimbo, Chile), 25/04/2015 (Mw7.8 Nepal). Fig.3 shows the most revealing ionograms during these earthquakes.

From Fig.3 one can see that sometimes the 'multicusp' effect is also accompanied by distortion and bifurcation of the F-track (Fig.3H2), that can

be interpreted as horizontal irregularities. More detailed ionogram dynamics for each earthquake response can also be found in the Support Information.

As it is shown by [Berngardt et al. (2015)], even for a powerful Tohoku 11/03/2011 earthquake the specific periods of perturbation and their amplitude can be evaluated under assumption of the monotony of the perturbed electron density profile. Therefore, to evaluate the perturbation amplitude we processed the ionograms by standard POLAN program (available at [POLAN Program ()]), which is traditionally used for multicusp analysis [Maruyama et al. (2011), Liu et al. (2013), Maruyama et al. (2016a), Maruyama et al. (2016b)].

For automatic processing of the data we developed a simple program set used to convert ionograms into profiles of plasma frequency. The automatic processing was easy to be done due to high quality of Irkutsk ionograms, already filtered out from neighboring public radiostations by original and very powerful technique [Podlesnyi et al (2014a)]. The algorithm for obtaining electron density profiles from ionograms consists of 3 stages. At the 1st stage, the ionogram is filtered out from rare dot-like noise of different nature. At the 2nd stage, the track is made over the data by dividing the frequency interval of significant signals into 50 subintervals, that is necessary for stable work of POLAN program. In each subinterval we find the median point over the height and frequency. At the 3rd stage the median points, collected over subintervals forms the 50-points track, are used as a source for POLAN calculations of plasma frequency profile.

Some results of this automatic processing are shown in Fig.4. In the figure the plasma frequency profiles are shown, and their differential over the frequency. From Fig.4 one can see that the main perturbations associated with multicusp can be observed from 140 km up to F2 maximum (for example, Fig.4A), so for their observations the ionosonde must operate in the appropriate mode, covering reflection heights from 100-140km to F2 maximum. As one can see, the surface seismic waves lead to formation of mid-scale short-lived plasma frequency variations that disturb initial, relatively smooth ionospheric profile. The amplitude of these effects is relatively small, and more evident at ionograms (that non-linearly depends on the plasma frequency profile), than in the plasma profile itself.

3.2 Sporadic E-layer bifurcation as possible effect of surface seismic waves

Another effect, that accompanied some of the earthquakes, was the change of sporadic E-layer structure, manifested in the form of bifurcation after the passage of the surface wave. Fig.5 shows an example of this effect for the

earthquake 07/12/2015 (Mw7.2 Tajikistan).

Fig.6A-C,E-G,I-K show the most characteristic ionograms for the earthquakes 25/10/2013 (Mw7.1 off east coast of Honshu, Japan), 16/02/2015 (Mw6.8 near east coast of Honshu, Japan), 07/12/2015 (Mw7.2 Tajikistan).

To emphasize this effect, we integrated amplitude at ionograms over frequency for each given effective height. This technique is close to the height-time-intensity(HTI) technique [Haldoupis et al. (2006)]. Dependence of the resulting amplitude on the effective height for different earthquakes (when we observe this effect) is shown in Fig.6D,H,L. The figure shows that the main effect is the appearance of an additional E-sporadic layer overlying the usual E-sporadic layer on the ionogram. It arises approximately 10-15 minutes after the passage of seismic disturbance at the point of observation and lasts about 20 minutes. After arising, the secondary reflection gradually decreases down to the height of the main E-sporadic track. At the same time with a decrease of the reflected signal height its amplitude is increased.

4 GPS-observations of IGWs near the earthquake epicenter

Examples of TEC variations in the vicinity of the epicenters of all considered earthquakes (Table 2) are shown in Fig.7. We selected the pairs "satellite-receiver" with rays closest to the earthquake's epicenter and with larger TEC effect (to take into account aspect dependence of TEC effects). The TEC variations at those rays are shown in Fig.7.

To estimate the efficiency of each earthquake for generating 2-10min TEC variations, we made a preliminary analysis of all the GPS data at the nearest GPS-stations. The results of the analysis are summarized in Table 2. The table also shows the local solar time of the main shock in the epicenter of the earthquake ("LST"), the focal mechanism of the earthquake ("Fault type") and background geomagnetic conditions on the day of the earthquake ("M.disturbance").

The information about focal mechanisms of the earthquake is obtained from the The Global CMT Project(<http://www.globalcmt.org>). The geomagnetic conditions are estimated from Dst and AE indexes, obtained from the International Data Centre in Kyoto (<http://wdc.kugi.kyoto-u.ac.jp/wdc>). In the table we mark the days with disturbed geomagnetic conditions ("disturbed") and with magnetic storms ($Dst < -50nT$, "storm"), based on the behavior of these indexes.

From the Table 2 one can see that during most part of the earthquakes the

geomagnetic conditions were quiet. So ionospheric irregularities related with geomagnetic disturbances has not prevent us to detect TEC-GPS response to earthquakes.

We classify TEC disturbances generated by the earthquakes into 3 following categories.

”Strong response” has relatively high amplitude (≥ 0.2 TECU) (Fig.7a,l,m,n,p) and recorded at many rays ”receiver-satellite”. Such responses are registered after five earthquakes: 11/03/2011, 25/04/2015, 26/04/2015, 12/05/2015, 16/09/2015. The magnitude of these earthquakes varies from 6.7 to 9.0, and all of them had reverse fault focal mechanism. It is important to note about very successful geometry of the measurements during all of these earthquakes: the most part of the ”receiver-satellite” rays were close to or directly above the epicenter.

In this category the most powerful earthquake 11/03/2011 (Tohoku, Japan) should be emphasized. It causes the most intense and prolonged ionospheric disturbances. Ionospheric effects of this earthquake are investigated in a huge amount of papers (see for example [Astafyeva et al. (2011), Liu et al. (2011), Nishitani et al. (2011)]). Recently, more attention is paid to modeling of these effects [Kherani et al. (2012), Kakinami et al. (2013), Shinagawa et al. (2013)] and to the study of the propagation of the disturbances at large distances [Jin et al. (2014), Bergardt et al. (2015), Tang et al. (2015)].

”Weak response” is the response that has relatively low amplitude (0.1-0.15 TECU) and recorded at several (2 to 5) rays ’satellite-receiver’. The shape and amplitude of such disturbances is high enough to detect it from the background TEC variations level.

In this category the deep earthquake 24/05/2013(Okhotsk Sea earthquake, Fig.7e) should be emphasized. It was very powerful earthquake (Mw8.3) with a predominance of vertical displacements in the epicenter (normal fault). It attracted the attention of seismologists, because felt at unusually large (10,000 km) distance from the epicenter [Ye et al. (2013), Zhan et al. (2014)]. The Earth’s surface displacement in the Sea of Okhotsk area caused by this earthquake were also studied using GPS-data [Steblov et al. (2014)]. However, due to the very large depth of the epicenter, the impact of the Okhotsk Sea earthquake to the ionosphere looks very weak. Perhaps that is why the ionospheric effects of the earthquake were not discussed too much in the literature. We could not find any work devoted to the GPS-TEC or ionospheric perturbations caused by this event on nearby region. During the present study we detected some TEC perturbations, most likely associated with the Okhotsk Sea earthquake, but only at two rays (MAG0-G06, MAG0-G16), closest to the epicenter of the earthquake.

”No response” category in the Table 2 means that we were unable to

identify any significant TEC disturbances related to the earthquake at any of the rays "receiver-satellite" (Fig.7 b, c). The effects were not observed after two earthquakes: 14/02/2013 and 16/04/2013. In our opinion the disturbance observed in 14/02/2013 (Fig.7b) is not a response to the earthquake, but should be associated with the intersection by the ray "receiver-satellite" by the sharp electron density gradient, perhaps the highlatitude trough. The analysis of the original (unfiltered) series of TEC variations leads us to this conclusion. As the analysis has shown, the series have a bend ("hook"), which is a characteristic for the cases when the beam crosses the steep gradient of the electron density, for example, the terminator or boundary of ionospheric trough. To "No response" category we also attributed the events when we detect a weak perturbations at one or two rays with the shape close to the shape associated with earthquake-generated perturbations usually [Calais and Minster (1995), Afraimovich et al. (2001a), Astafyeva et al. (2009), Astafyeva et al. (2013), Perevalova et al. (2014), Perevalova et al. (2015)] (Fig.7 d, k). However, due to a number of reasons (the absence of such disturbances on the other rays, a significant propagation velocity exceeding sound speed, etc.) there is no assurance that these perturbations can be caused by an earthquake (for example, in case of 20/04/2013 and 20/04/2015).

No GPS-TEC response to the earthquake may have several causes. First of all, the earthquakes with small magnitude and with predominance of horizontal displacement in the focus (strike-slip faults) that produce very small effects with amplitudes lower than background effects. As it was shown in [Perevalova et al. (2014)], after the earthquakes with magnitudes $Mw < 6.5$ appreciable TEC wave-like disturbances are not observed, and in the case of strong earthquakes ($Mw > 6.5$) responses are more pronounced after the events with substantial vertical component in the focus (normal or reverse fault). Another important cause is the geometry of GPS-measurements. In most cases, the lack of response at the beam path "receiver-satellite" may be related with a large distance from the ionospheric point to the epicenter (the mark "rays far away" in Table 2).

For "strong response" and "weak response" categories we estimated the propagation velocity of disturbances. The estimate is done for the first impulse response. The velocity V is calculated from a simple linear propagation model $V = dS/dt$, where dS is the line-of-sight distance between the epicenter and the ionospheric point at which the response was recorded, dt is the delay between the TEC variation maximum moment and the moment of the earthquake (shown in Table2). The resulting values of V are summarized in Table 2. The calculated propagation velocity varies between 150 and 600 m/s. This indicates that these perturbations can be associated with propagation of internal atmospheric waves [Shinagawa et al. (2007), Occhipinti et al. (2008),

Matsumura et al. (2011), Kherani et al. (2012)].

5 Discussion

5.1 Class of Reyleigh wave acoustical efficiency K_W

As the analysis of GPS-TEC measurements shows above, near the epicenter the most part of earthquakes were accompanied by TEC-variations (see Fig.8A). From the other side, the multicusp effect at large distances accompanies only several earthquakes.

So the question naturally arises, how can we estimate the effectiveness of a given surface seismic wave for the formation of those or other effects in the ionosphere. To estimate this, we introduce the class of Rayleigh wave acoustical efficiency (RWAEC) that is determined by the amplitude of the local seismic vibrations below the point of ionospheric observations.

It can be shown that for distributed acoustic wave source the Mach cone amplitude $A_{acoustic}$ can be estimated by multiplying Mach cone amplitude from moving point source to the acoustic radiation pattern of distributed source:

$$A_{acoustic} \approx G_{Mach} \cdot g\left(\alpha \sin\left(\frac{C_s}{V_{Rayleigh}}\right)\right) \quad (1)$$

where G_{Mach} is the amplitude of acoustic signal in the shock wave, generated by dot-like (isotropic) acoustic source moving with supersonic speed; $g(\alpha)$ is the acoustic radiation pattern of the distributed source itself as a function of zenith angle α , calculated from relation between sound speed C_s and supersonic source speed $V_{Rayleigh}$ (supposed to be 3.5km/s).

The radiation pattern $g(\alpha)$ is defined by the spatial structure of the propagating seismic wave. This approximation does not take into account the phase radiation pattern. The exact spatial wave structure is unknown for us, but we can assume that the wave has some spatial shape, that moves without dispersion with the supersonic speed of seismic wave.

Based on this approximation we can use temporal variations of the seismic signal at a given station to estimate the spatial shape of an equivalent acoustic source. In this case we can calculate the radiation pattern associated with the spatial distribution of seismic oscillations, and estimate the amplification of the Mach cone as a function of seismic signal shape. It should be noted that since the seismic wave velocity is much higher than acoustic sound speed in the atmosphere, one needs to take into account the radiation pattern

only at the angles close to the perpendicular to the Earth's surface (i.e. perpendicular to the radiation plane).

The principle of the formation of a Mach cone with taking into account the acoustic signal radiation pattern is illustrated in Fig.8B.

The intensity of the acoustic signal in the far zone of the acoustic antenna (that is approximately valid for this case) is defined by radiation pattern. The radiation pattern $g(\vec{k})$ of distributed sound source in its far field zone is defined [Smaryshev (1973)] as:

$$g(\vec{k}) = \int \Omega(\vec{r}) e^{i \vec{k} \cdot \vec{r}} d\vec{r} \quad (2)$$

where $\Omega(\vec{r})$ is vibrational velocity of the sound source (we suppose the movements to be strictly vertical). In one-dimensional, steady-state case, we can estimate the vertical velocity of the surface oscillations from the experimental data as

$$\Omega(r) = \left\{ \frac{\tilde{h}(t)}{dt} \right\}_{t=(r-r_0)/V_{seismo}} \quad (3)$$

In this case, the wave vector of the radiation \vec{k} is close to the perpendicular to the plane of the source \vec{r} and their scalar product is small. In the one-dimensional case, for plain Earth approximation, along the direction of the Rayleigh wave motion (this case corresponds to a significant distance between observation point and the epicenter of the earthquake, when the seismic wave can be considered having not spherical but plane front), the acoustic radiation pattern can be estimated from one-dimensional spectrum:

$$g(\vec{k}) = i k_{eff} V_{seismo} \int \tilde{h}(r) e^{i k_{eff} r} dr \quad (4)$$

where $k_{eff} = \vec{k} \cdot \frac{\vec{r}}{r}$ is a wavenumber projection to the acoustic source plane.

Fig.8C shows examples of radiation pattern, calculated for Tohoku (11/03/2013) earthquake for two wavelengths - $\Lambda = 1km$ (black line) and $\Lambda = 10km$ (red line), as a function of zenith angle. The dashed line marks the direction of shockwave propagation. As one can see, the antenna pattern is different for different wavelengths. So we can find the wavelength, for which the amplitude of acoustical signal becomes maximal in shockwave direction. The amplitude corresponds to the maximum of the spectrum (3). So searching the wavelength most effective for generating acoustical signal in the first approximation corresponds to the search of maximum in the spectrum (3).

Thus, for fixed height of the expected effect R and excluding the effects of the sound propagation in the neutral atmosphere and the energy transformation from the neutral component to the charged one, the spectral energy class of the acoustic signal caused by seismic vibrations can be estimated from the maximal amplitude of radiation pattern, and consequently from the spectrum of the derivative of seismic vibrations like:

$$K_w = \log_{10} \left\{ \max \left\{ \left| \frac{\omega}{2\pi} \int_T \tilde{h}(t) e^{-i\omega t} dt \right|^2 \right\} \right\} - 10 \quad (5)$$

where \tilde{h} in nanometers. For calculating the spectrum in (5) we used 8192 and 16384 point fast Fourier transform. Fig.8D shows a comparative analysis of the spectra of the derivative of the vertical vibrations during several earthquakes (11/03/2011, 24/05/2013 and 12/05/2015) that are close in Irkutsk local solar time, as well as close in season. One can see that the spectra (and acoustic radiation patterns) differs significantly, and this can explain the difference in the amplitude of the effect, observed in the ionosphere.

5.2 Statistical dependences

The Fig.8E and Table 3 summarize the main effects of earthquakes observed by IFMCI as a function of local solar time and Rayleigh wave acoustic efficiency class K_W . One can see from the Fig.8E that at night multicusp effect is not observed. This can be due to the fact that for nighttime low electron density the standard ionograms start from 250km altitude. For relatively weak $K_W < 3.6$ multicusp is not observed even in the daytime. For relatively high $K_W \geq 4.8$ multicusp is observed nearly regularly at daytime [07:00-17:00]LST. It should be noted that at the 16:00 and 01:00 LST multicusp is not observed, although tracks observed at ionograms allow us to detect such effect. We can make a conclusion that to observe multicusp in the F-layer is too difficult at night. This can be explained qualitatively by the need of more energy for seismic oscillations at nighttime to generate waves in high F-layer than at daytime to generate the effects in the lower F1 or E-layer. This is due to the fact that lower electron density produces less neutral-electron collisions, that are the main agents for energy transfer from neutral acoustic wave to electron density variations [Chum et al. (2012), Laštovička (2006), Maruyama and Shinagawa (2014)].

To verify our conclusions about the power and daily features of multicusp

observations we also analyzed the results from some of the most detailed papers. In particular, we calculated K_W index for the observations of ionospheric multicusp reported in ([Chum et al. (2016), Maruyama et al. (2016a), Liu et al. (2011)]). The calculation of K_W was made from the seismic vibrations observed at seismic stations nearby the locations of observed ionospheric effects (the ARU seismic station (Sverdlovsk region, Russia), TATO seismic station (Taiwan) and NKC seismic station (Czech Republic)). The results are also summarized in the Table 3 and Fig.8E. These cases are marked by asterisks and confirm the obtained results.

In the morning, evening and night time ($LST > 15:00, LST < 07:00$) we observed cases of bifurcation effect in the sporadic E-layer. This track separation can be explained by the formation of an additional horizontal layer above the regular sporadic-E that causes the appearance of an additional reflection point. One can assume several variants of how to explain the observed bifurcation effect in the sporadic E-layer.

We assume that we observe a downward movement of irregularities due to translucency of sporadic E-layer, by analogy with [Haldoupis et al. (2006), Haldoupis (2012)]. In this case, the downward movement occurs with nearly wind speeds.

The presented observations of GPS-TEC disturbances in the vicinity of earthquake epicenters confirm the data obtained in previous studies [Perevalova et al. (2014), Astafyeva et al. (2013)]. With the increasing of the earthquake magnitude, in general, an increase in TEC amplitude perturbations is observed as well. The TEC response is also affected by the mechanism of the earthquake source: after the earthquake, in the epicenter of which a vertical displacements are dominated, the TEC variations are intensified and are detected at a large number of rays "satellite-receiver". The geometry of measurements also plays an important role: the absence of rays "satellite-receiver" near the epicenter makes it difficult to detect responses even after earthquakes with magnitudes $M_w > 7$. It may also be noted that after strong earthquakes ($M_w > 8$), in addition to the first pulse associated with the main shock, a number of secondary vibrations is observed. They are caused, in our opinion, by the generation of eigen oscillations of the atmosphere with different periods (IGWs) [Lognonné et al. (1998), Artru et al., (2001)].

The dependence of TEC effects on the local time has not been identified (see Table2). The diurnal variation of effects suggests that generation of IGWs more likely do not depend on the local time. The dependence of intensity of IGWs effects on the nature of earthquakes was discussed, for example, in [Astafyeva et al. (2014)].

This means that the found dependence of multicusp from the local time that is not detected in the epicenter vicinity. It significantly depends on the

specific mechanism of multicusp generation by the shock wave. This can be qualitatively explained by the dependence of the ion-neutral collisions mechanism on the product of the background neutral density and background electron density, that is maximal in a daytime.

6 Conclusion

In the paper the statistical analysis of ionospheric effects of earthquakes that occurred in 2011-2016 according to the Irkutsk fast monostatic chirp ionosonde was made. To control the process of neutral-ionospheric interaction in the vicinity of epicenter the data from GPS-receivers were also analyzed for each of these earthquakes.

To estimate the ionospheric efficiency class for seismic disturbances in the far field of epicenter, that cause propagation of the shock cone (Mach cone) we proposed the logarithmic index K_W (5), based on finding the maximal amplitude of spectral power fluctuations. From a physical point of view, the index allows us to estimate the maximal amplitude of the shock wave (Mach cone) based on spatial distribution of seismic oscillations and their vertical velocities. So the index depends on the amplitude of the acoustic effects associated with the passage of seismic surface wave. The analysis shows that the characteristic index value, from which IFMCI can see multicusp effect in the ionosphere (at daytime [7:00-17:00]LST $K_W \geq 4.7$). The bifurcation of sporadic E-layer can be observed at nighttime at $K_W > 3.6$.

It is shown that a multicusp effect according IFMCI data has a rather pronounced daily dependence, intensified in local daytime hours, with absence of characteristic dependence on foF2. This allows us to suggest that the possibility of observing the effect is likely due not to the intensity of the primary F2 layer, but due to other mechanisms at lower heights. It is shown that when ionograms start above 250km (in the morning, evening and night) the multicusp effect in Irkutsk is not observed, this corresponds well with results of [Chum et al. (2016)].

It is shown that this effect is not associated with daily dependence of the generation of ionospheric disturbances in the vicinity of the earthquake epicenter, estimated by GPS data. This suggests that the efficiency of generation of irregularities on the Mach shock wave and in the vicinity of earthquake epicenter are apparently different.

On the example of deep earthquake in the Okhotsk Sea (25/10/2013, depth about 600 km) it can be assumed that the effects of Rayleigh wave in the case of deep earthquakes may be more noticeable than IGW effects in the vicinity of earthquake epicenter. Thus, in spite of the daily dependency

effects, the effects from Rayleigh waves are an additional way to study the ionospheric response to earthquakes, because they can sometimes produce more strong effects than IGWs generated in the epicenter.

It is shown that after passing the Rayleigh wave sometimes can be observed a bifurcation in sporadic E-layer, observed as secondary E-layer arised and moving downward to basic sporadic E. This can be associated with formation of vertical irregularities and their dynamics under the influence of the dynamics of the neutral atmosphere.

As a result of the work it is shown that fast IFMCI is a very sensitive instrument for investigating of rapid ionospheric effects related to the earthquakes with $K_W \leq 3.6$ during the day, which roughly corresponds to the characteristic magnitudes of distant earthquakes above $M \geq 6.5$. This makes the ionosonde a convenient tool for the diagnosis of various processes that occur during seismo- ionospheric interaction.

The obtained results allow us to suggest K_W and local solar time as effective parameters for searching the multicusp effects in the ionosphere related with surface seismic waves.

7 Acknowledgments

We are grateful to ISTP SB RAS stuff: to Dr. Lebedev V.P. and Dr. Tashilin A.V. for fruitful discussion, to Ivanov D.V. and Salimov B.G. for preparing ionograms for analysis.

We are grateful to Scripps Orbit and Permanent Array Center (SOPAC) for the provision of data from the global network of GPS receivers.

We are grateful to IRIS/IDA Seismic Network (II), Global Seismograph Network (GSN - IRIS/USGS) (GSN,IU), SY - Synthetic Seismograms Network (SY) for providing seismic data.

Irkutsk fast monostatic chirp ionosonde data is property of ISTP SB RAS, contact Oleg I. Berngardt (berng@iszf.irk.ru). The functionality of IFMCI was supported by FSR program #II.12.2.3.

The work was done under financial support of the project #0344-2015-0019 "Study of the lithosphere-atmosphere-ionosphere system in extreme conditions" of the program of Presidium of RAS, grant NSH-6894.2016.5 of the President of State Support for Leading Scientific Schools.

K_A	Date/time	Epicenter	Depth	M	Location
17	2011-03-11 05:46:23.0	38.30N,142.50E	22	9.0	Honshu, Japan (Tohoku)
16	2012-02-26 06:17:19.0	51.72N,95.99E	10	6.6	Southwestern Siberia, Russia
12	2012-04-11 08:38:35.0(a)	2.37N,93.17E	10	8.4	Northern Sumatra
8	2012-04-11 10:43:09.0(b)	0.81N,92.45E	10	8.0	Northern Sumatra
7	2012-12-07 08:18:23.0	37.92N,144.02E	30	7.3	Honshu, Japan
11	2013-02-14 13:13:53.0	67.62N,142.66E	10	6.6	Sakha, Russia
10	2013-04-16 10:44:20.0	28.14N,62.08E	87	7.8	Iran-Pakistan border
13	2013-04-20 00:02:48.7	30.33N,102.99E	20	6.6	Sichuan, China
14	2013-05-24 05:44:48.0	54.91N,153.34E	598	8.3	Okhotsk Sea
13	2013-09-24 11:29:49.0	27.07N,65.56E	20	7.7	Pakistan
8	2013-09-28 07:34:06.0	27.24N,65.56E	10	6.8	Pakistan
10	2013-10-25 17:10:17.0	37.22N,144.69E	10	7.1	Honshu, Japan
8	2014-04-12 20:14:37.0	11.26S,162.26E	10	7.6	Solomon Islands
8	2015-02-16 23:06:27.4	39.87N,142.94E	15	6.8	Honshu, Japan
6	2015-04-20 01:42:55.5	24.21N,122.52E	7	6.4	Taiwan Region
16	2015-04-25 06:11:26.9	28.24N,84.74E	15	7.8	Nepal
8	2015-04-26 07:09:10.3	27.86N,86.08E	15	6.7	Nepal
12	2015-05-12 07:05:19.0	27.89N,86.17E	10	7.3	Nepal
15	2015-09-16 22:54:31.8	31.55S,71.58W	20	8.3	Coquimbo, Chile
15	2015-09-17 23:18:43.1	31.55S,71.68W	40	7.0	Coquimbo, Chile
11	2015-10-26 09:09:32.0	36.48N,70.91E	207	7.5	Hindu Kush, Afghanistan
8	2015-11-13 20:51:35.2	30.95N,129.00E	10	6.7	Kyushu, Japan
12	2015-12-07 07:50:07.2	38.18N,72.91E	30	7.2	Tajikistan
7	2016-01-30 03:25:09.8	54.03N,158.54E	159	7.2	Kamchatka, Russia
13	2016-03-02 12:49:48.0	4.89S,94.25E	20	7.8	Sumatra, Indonesia
11	2016-04-15 16:25:07.3	32.85N,130.57E	10	7.0	Kyushu, Japan
8	2016-04-16 23:58:37.2	0.40N,79.89W	20	7.8	Ecuador
10	2016-07-29 21:18:30.2	18.58N,145.51E	267	7.7	N. Mariana Islands

Table 1: List of seismic disturbances, participated in the analysis, and the corresponding earthquake (according to the European-Mediterranean Seismological Centre <http://www.emsc-csem.org>).

References

- [Afraimovich et al. (2000)] Afraimovich E.L. (2000) GPS global detection of the ionospheric response to solar flares *Radio Science* 35(6):1417–1424
- [Afraimovich et al. (2001a)] Afraimovich, E. L., Perevalova, N. P., Plotnikov, A. V., and Uralov, A. M. (2001a). The shock-acoustic waves generated by earthquakes. *Annales Geophysicae*, 19(4):395–409.
- [Afraimovich et al. (2001b)] Afraimovich, E.L., Kosogorov, E.A., Lesyuta, O.S., Yakovets, A.F., Ushakov, I.I.(2001b) Geomagnetic control of the spectrum of traveling ionospheric disturbances based on data from a global GPS network *Ann. Geophys* 19(7):723–731
- [Akchurin et al. (2011)] Akchurin A.D., Bochkarev V.V., Ildiryakov V.R., Usupov K.M. (2011) TID selection and research of its characteristics on ionograms *30th URSI General Assembly and Scientific Symposium. Istanbul, 2011*. GP1.23.
- [Artru et al., (2005)] Artru, J., Ducic, V., Kanamori, H., Lognonné, P., and Murakami, M. (2005). Ionospheric detection of gravity waves induced by tsunamis. *Geophysical Journal International*, 160:840–848.

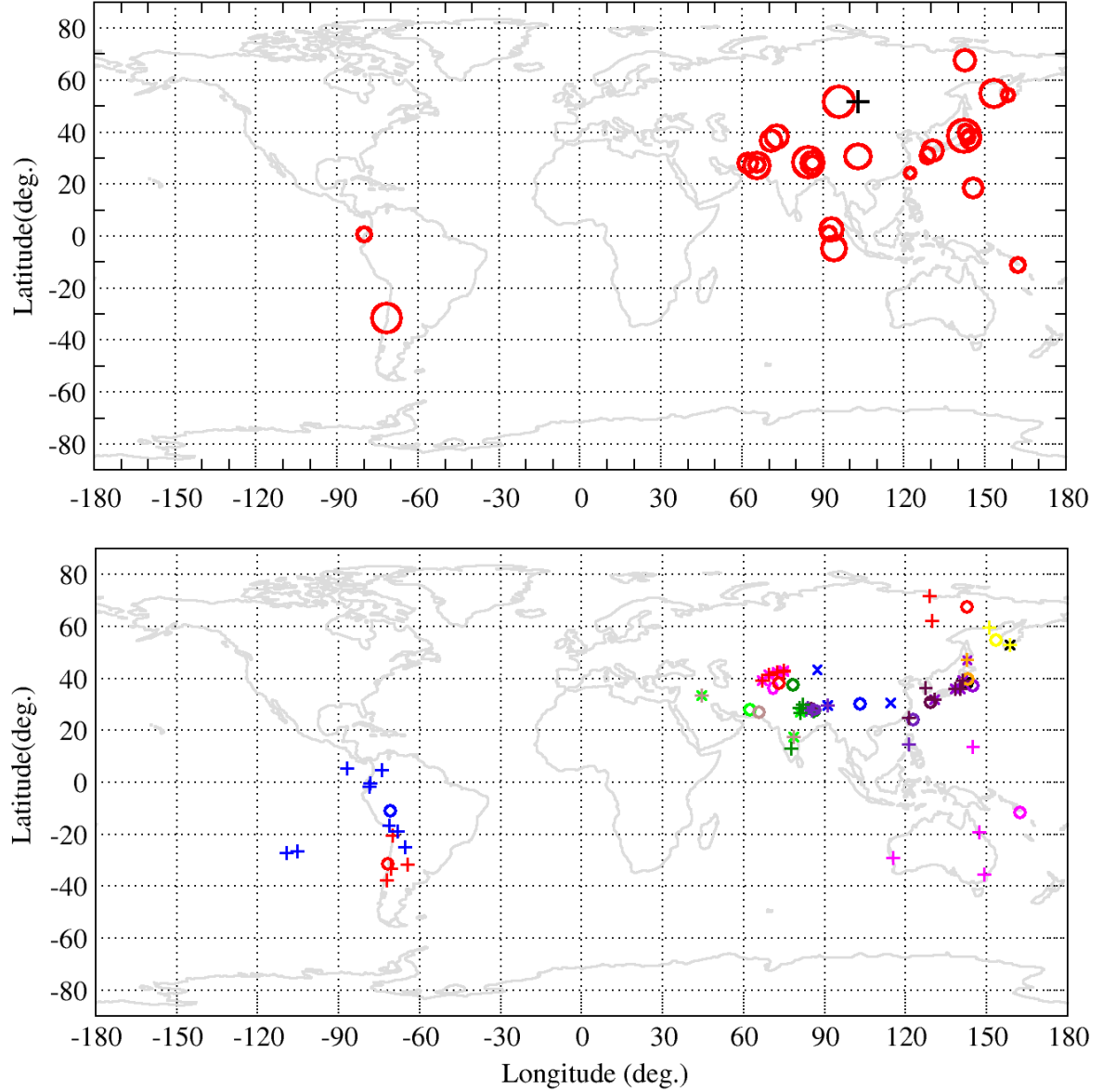


Figure 1: A) Geometry of chirp measurements in 2011-2016. Circles correspond to earthquakes epicenters, their radii corresponds to calculated K_A . Cross corresponds to measurement location (IFMCI and TLY seismic station). B) Geometry of GPS measurements in 2013-2015. Circles correspond to earthquakes epicenters, crosses and diagonal crosses correspond to the GPS stations. The same colors of circle and crosses correspond to the same event.

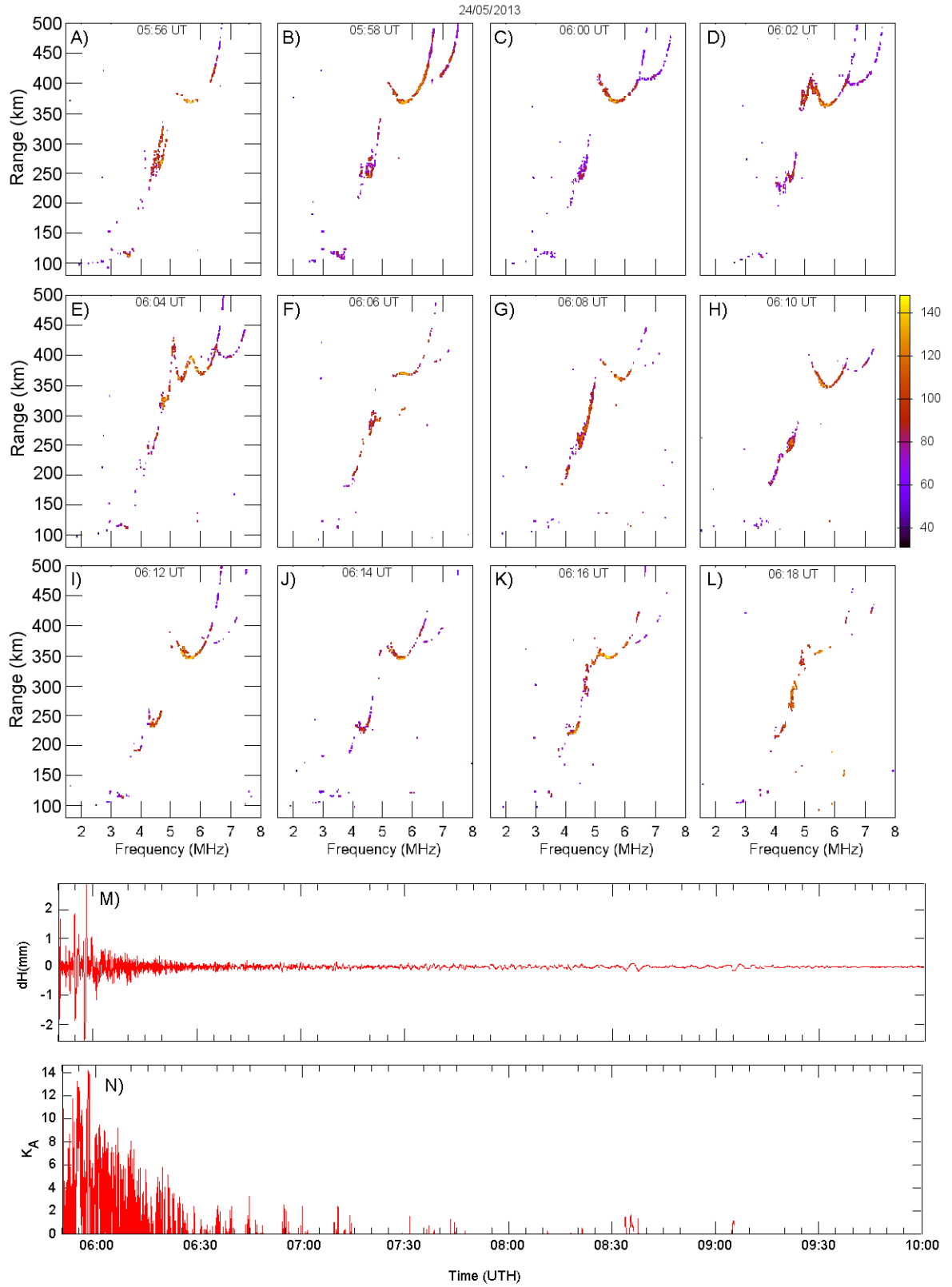


Figure 2: An example of the ionospheric dynamics related to the passage of the seismic wave at ionograms from IFMCI (after Okhotsk Sea earthquake, 24/05/2013). A-L) - consequent ionograms shown every 2 minutes; M) - TLY seismic vertical variations; N) - K_A variations.

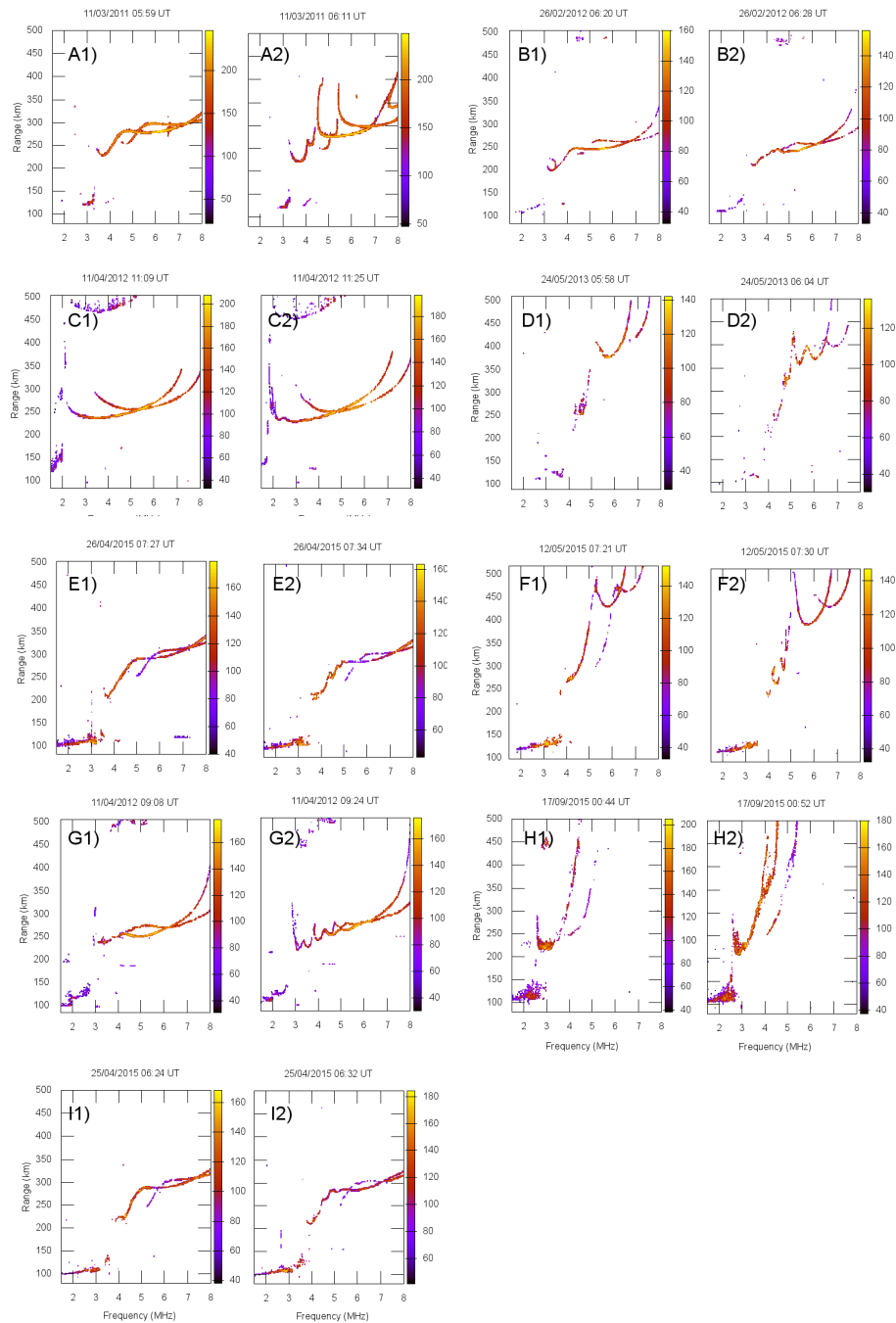


Figure 3: Multicusp ionograms during earthquakes A1,2) 11/03/2011 (Mw9.0 Tohoku, Japan), B1,2) 26/02/2012 (Mw6.6 Southwestern Siberia, Russia), C1,2) 11/04/2012 (Mw8.4 Northern Sumatra), D1,2) 24/05/2013 (Mw8.3 Okhotsk Sea), E1,2) 26/04/2015 (Mw6.7 Nepal), F1,2) 12/05/2015 (Mw7.3 Nepal) G1,2) 11/04/2012 (Mw8.0 Northern Sumatra) H1,2) 17/09/2015 (Mw8.3 Coquimbo, Chile) I1,2) 25/04/2015 (Mw7.8 Nepal) . Quiet and disturbed profiles marked by 1 and 2 correspondingly.

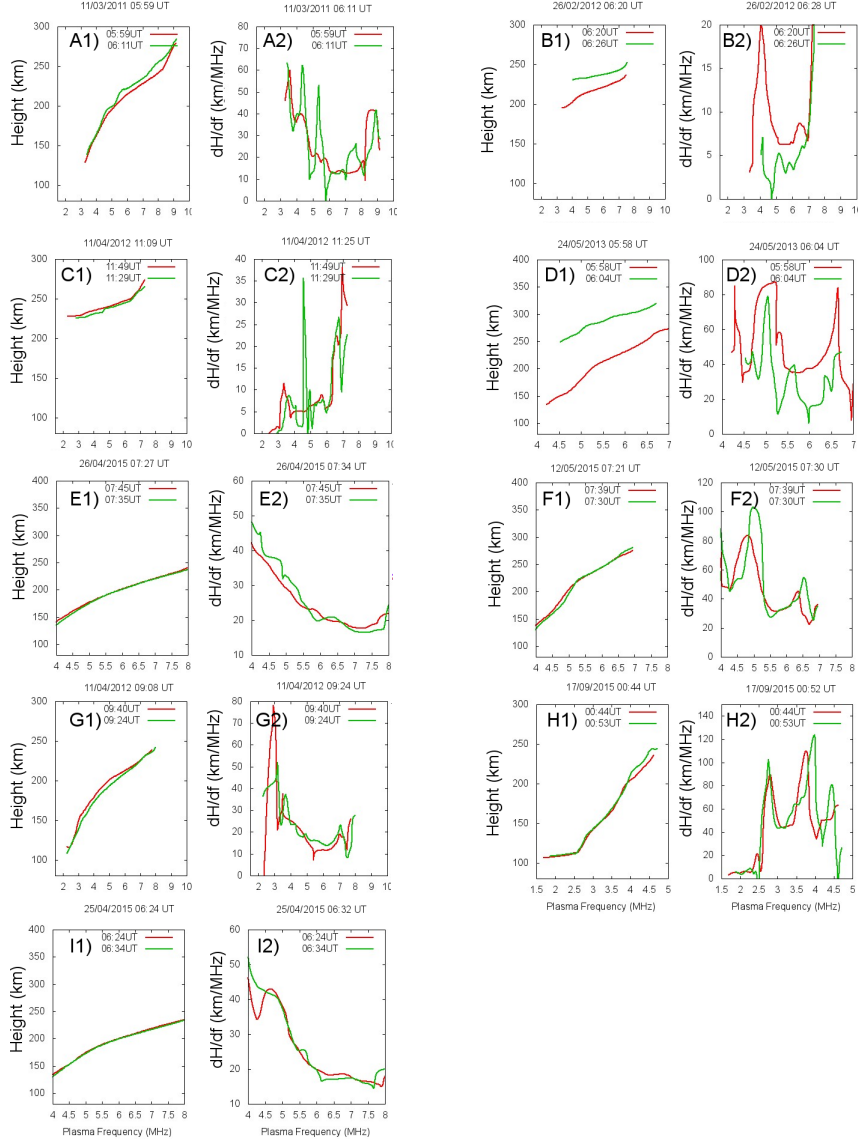


Figure 4: Multicusp profiles during earthquakes A1,2) 11/03/2011 (Mw9.0 Tohoku, Japan), B1,2) 26/02/2012 (Mw6.6 Southwestern Siberia, Russia), C1,2) 11/04/2012 (Mw8.4 Northen Sumatra), D1,2) 24/05/2013 (Mw8.3 Okhotsk Sea), E1,2) 26/04/2015 (Mw6.7 Nepal), F1,2) 12/05/2015 (Mw7.3 Nepal) G1,2) 11/04/2012 (Mw8.0 Northen Sumatra) H1,2) 17/09/2015 (Mw8.3 Coquimbo, Chile) I1,2) 25/04/2015 (Mw7.8 Nepal) . Quiet and disturbed profiles marked by red and green correspondingly. 1 and 2 marks height(1) and height derivative(2) correspondingly.

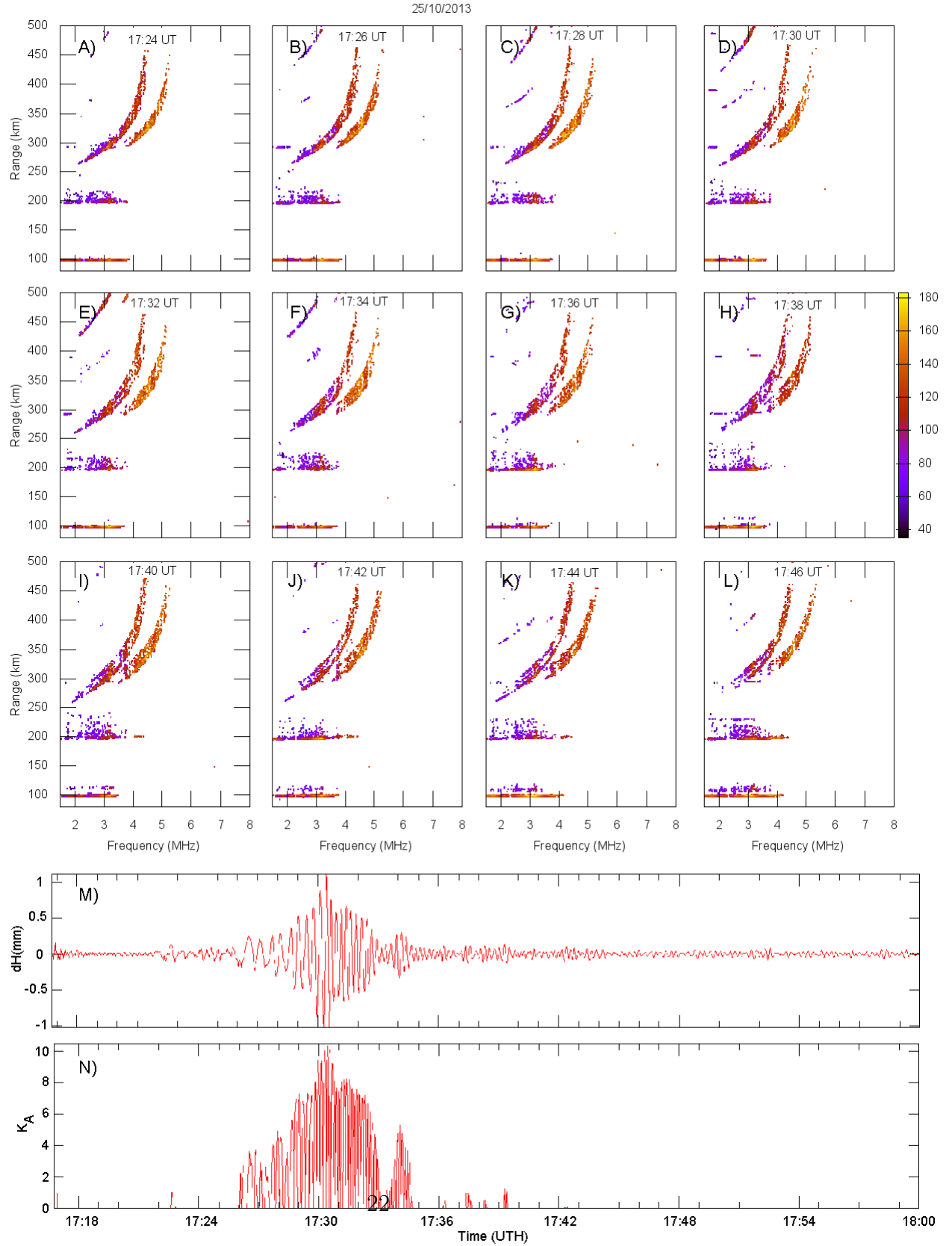


Figure 5: Bifurcation effect in E-sporadic layer after Honshu earthquake 25/10/2013. A-L) - consequent ionograms shown every 2 minutes; M) - TLY seismic vertical variations; N) - K_A variations.

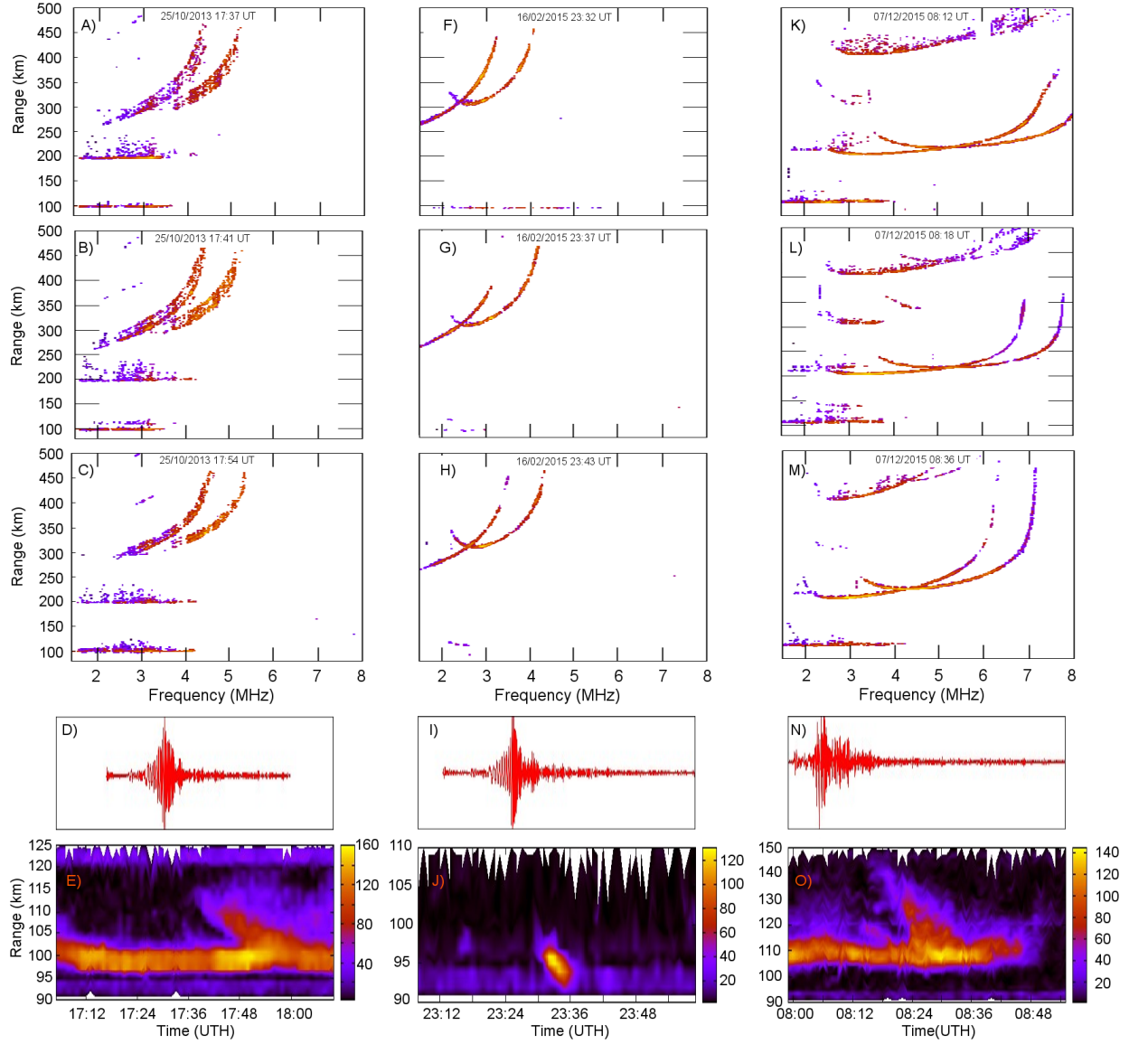


Figure 6: The effect of sporadic E bifurcation observed in experiments, 25/10/2013 (A-E), 16/02/2015(F-J), 07/12/2015(K-O). A,B,C, F,G,H, K,L,M - ionograms; D,I,N - TLY vertical seismic variations; E,J,O - Intensity of chirp signal reflected from different heights, as a function of the time.

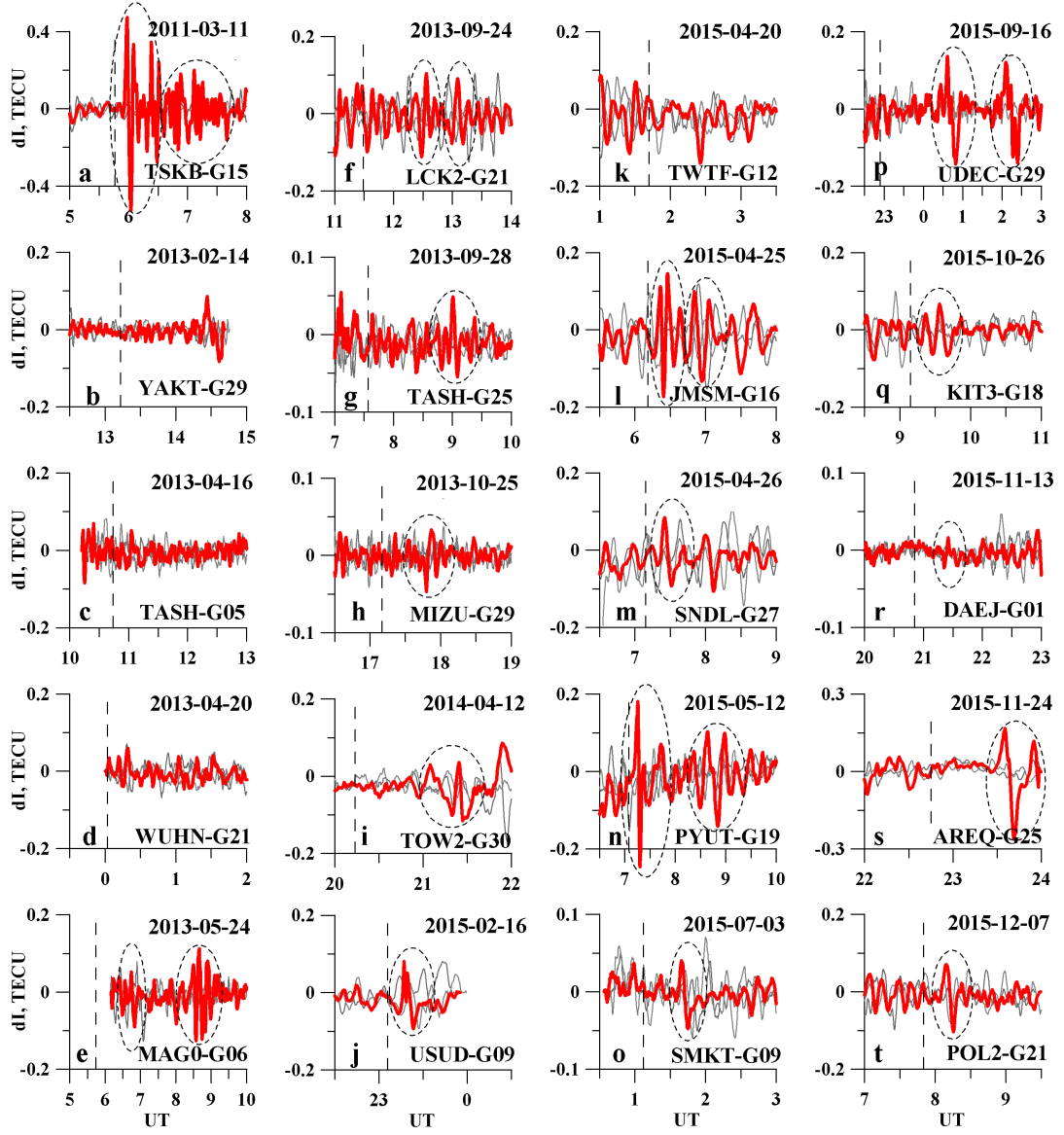


Figure 7: Examples of GPS-TEC disturbances in the vicinity of earthquake epicenters. The red lines show the variation of the TEC in the day of the earthquake, gray - the previous and subsequent days. The vertical dashed line marks the moment of the earthquake. The dashed ellipses mark disturbances caused by earthquakes.

EQ date	UT	M	LST	M.disturbance	Fault type	V(m/s)	Effect
2011-03-11	05:46:23	9.0	15.267	AE disturb.	reverse	535	strong response
2013-02-14	13:13:53	6.6	22.728	quiet	reverse+strike-slip	-	no response
2013-04-16	10:44:20	7.8	14.872	quiet	normal+strike-slip	-	no response, rays far away
2013-04-20	00:02:48	6.6	6.899	quiet	reverse+strike-slip	-	no response, rays far away
2013-05-24	05:44:48	8.3	15.956	quiet	normal	165	weak response
2013-09-24	11:29:49	7.7	15.854	AE disturb.	strike-slip	368	weak response, rays far away
2013-09-28	07:34:06	6.8	11.938	quiet	strike-slip	316	weak response
2013-10-25	17:10:17	7.1	2.813	quiet	normal	152	weak response
2014-04-12	20:14:37	7.6	7.05	Dst storm	normal	304	weak response, rays far away
2015-02-16	23:06:27	6.8	8.629	Dst storm	reverse	460	weak response
2015-04-20	01:42:55	6.4	9.868	Dst disturb.	reverse	-	no response
2015-04-25	06:11:26	7.8	11.83	quiet	reverse	505	strong response
2015-04-26	07:09:10	6.7	12.889	quiet	reverse	394	strong response
2015-05-12	07:05:19	7.3	12.828	AE disturb.	reverse	525	strong response
2015-07-03	01:07:46	6.4	6.324	quiet	reverse	286	weak response
2015-09-16	22:54:31	8.3	18.128	AE disturb.	reverse	145	strong response
2015-10-26	09:09:32	7.5	13.877	quiet	reverse	423	weak response
2015-11-13	20:51:35	6.7	5.45	quiet	strike-slip	296	weak response
2015-11-24	22:45:40	7.6	18.01	quiet	normal	165	weak response
2015-12-07	07:50:07	7.2	12.69	AE disturb.	strike-slip	443	weak response

Table 2: Results of the GPS-TEC observations in the vicinity of earthquake epicenter as well as parameters of the earthquakes and space weather disturbance level in 2013-2015.

Date	K_W	S.station	Period (sec)	LST	foF2 (MHz)	M	Effect
25/04/2015*	8.8	TATO	13.7	14.6	14.5*	7.8	*m/h 250km, no effect[Chum et al. (2016)]
11/03/2011*	8.0	TATO	22.7	14.0	11*	9.0	*Multicusp[Liu et al. (2011)]
11/03/2011	6.6	TLY	7.9	13.0	9	9.0	Multicusp
27/02/2010*	5.8	ARU	11.3	11.2	7*	8.8	*Multicusp[Maruyama et al. (2016a)]
11/04/2012(a)	5.7	TLY	17.6	16.2	8.5	8.4	Multicusp
24/09/2013	5.7	TLY	8.0	18.9	7	7.7	no effect
24/05/2013	5.6	TLY	25.2	13.0	7	8.3	Multicusp
25/04/2015	5.6	TLY	10.9	13.5	9.5	7.8	Multicusp
17/09/2015	5.4	TLY	11.4	7.3	4.2	7.0	Multicusp
16/04/2013	5.2	TLY	16.5	18.1	8.5	7.8	Disturbed conditions
11/04/2012(b)	5.1	TLY	11.2	18.3	7.5	8.0	Multicusp
25/10/2013	5.1	TLY	7.4	0.5	4.5	7.1	Esp bifurcation
12/05/2015	4.9	TLY	11.7	14.4	7	7.3	Multicusp
25/04/2015*	4.8	NKC	17.2	07.8	7.5*	7.8	*Multicusp[Chum et al. (2016)]
12/04/2014	4.8	TLY	7.9	3.9	4	7.6	m/h 270km, no effect
16/09/2015	4.8	TLY	8.5	6.3	4	8.3	Disturbed conditions
26/02/2012	4.7	TLY	7.3	13.3	8.0	6.6	Multicusp
14/02/2013	4.7	TLY	41.9	20.5	4.2	6.6	m/h 250km, no effect
07/12/2015	4.6	TLY	3.2	15.1	7	7.2	Esp bifurcation
02/03/2016	4.5	TLY	9.9	20.4	5.0	7.8	no effect
20/04/2013	4.4	TLY	7.1	7.3	7	6.6	Disturbed conditions
17/04/2016	4.4	TLY	10.7	8.3	4	7.8	Disturbed conditions, no effect
07/12/2012	4.2	TLY	7.6	15.6	7.0	7.3	no effect
28/09/2013	4.2	TLY	8.8	15.0	8	6.8	no effect
16/02/2015	4.2	TLY	6.0	6.4	3	6.8	Esp bifurcation, m/h 250km
26/10/2015	4.2	TLY	54.6	16.4	8	7.5	no effect
15/04/2016	4.2	TLY	53.1	23.7	4	7.0	Disturbed conditions
29/07/2016	4.1	TLY	62.4	4.7	3.5	7.7	Disturbed conditions, no effect
26/04/2015	3.6	TLY	5.0	14.4	9	6.7	Multicusp
13/11/2015	3.5	TLY	13.2	4.1	3.5	6.7	no effect, m/h 250km
20/04/2015	3.2	TLY	7.6	9.1	9.2	6.4	no effect
30/01/2016	3.1	TLY	273.4	10.7	8.0	7.2	Disturbed conditions

Table 3: Earthquakes on Rayleigh efficiency classes K_W . Asterisks denote effects according to other publications with the calculated coefficients over the data from corresponding seismic stations in the vicinity of observation point. m/h defines the minimal observed height of F-track at the ionogram. (*) Asterisk marks the data, available from some other publications.

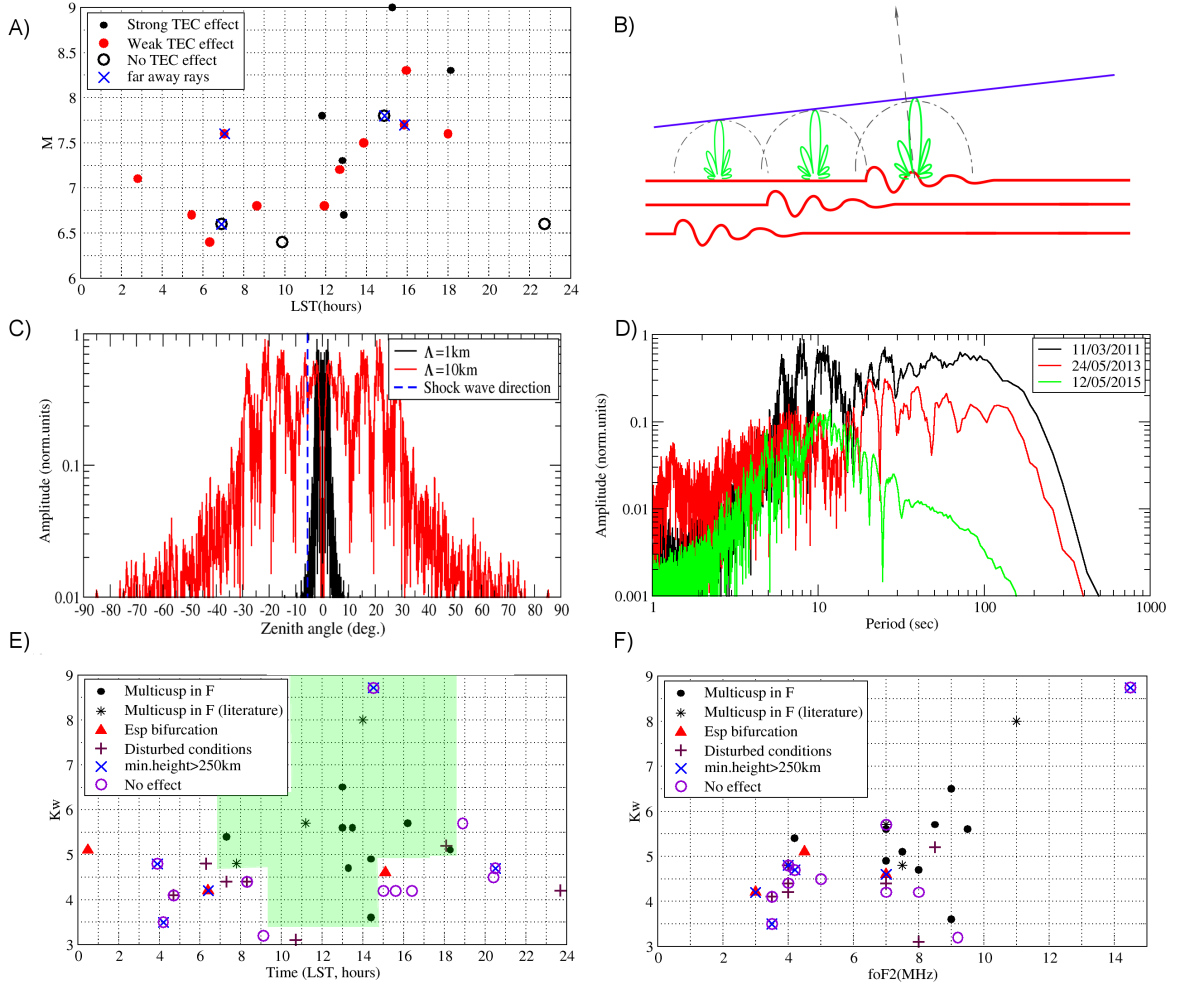


Figure 8: A) The ionospheric effects of earthquakes in the vicinity of epicenter detected by TEC-GPS technique, as function on the earthquake magnitude and local solar time; B) Scheme of shockwave (Mach cone) formation with taking into account acoustic radiation pattern. C) Intensity of acoustic wave as a function of zenith angle (acoustic radiation pattern). Calculated from TLY vertical seismic oscillations for 11/03/2011 (Tohoku) earthquake. Red line corresponds to 10 km wavelength, black line - to 1 km wavelength. Blue dashed line corresponds to the zenith angle of shockwave propagation. D) The spectrum of seismic oscillations for earthquakes producing multicusp in Irkutsk. E) Types of observed ionospheric effects related with surface seismic waves in 2011-2016 as a function of local time and acoustic efficiency class K_W . Green area marks the area with all the multicusps observed. F) Types of ionospheric responses as a function of $foF2$ and acoustic efficiency class K_W .

- [Artru et al., (2004)] Artru, J., Farges, T., and Lognonné, P. (2004). Acoustic waves generated from seismic surface waves: propagation properties determined from Doppler sounding observations and normal-mode modelling. *Geophysical Journal International*, 158:1067–1077.
- [Artru et al., (2001)] Artru, J., Lognonné, P., and Blanc, E. (2001). Normal modes modelling of post-seismic ionospheric oscillations. *GRL*, 28:697–700.
- [Astafyeva et al. (2009)] Astafyeva, E., Heki, K., Kiryushkin, V., Afraimovich, E., and Shalimov, S. (2009). Two-mode long-distance propagation of coseismic ionosphere disturbances. *Journal of Geophysical Research (Space Physics)*, 114(a13):10307.
- [Astafyeva et al. (2011)] Astafyeva, E., Lognonné, P., and Rolland, L. (2011). First ionospheric images of the seismic fault slip on the example of the Tohoku-Oki earthquake. *Geophysical Research Letters*, 38(22):L22104
- [Astafyeva et al. (2014)] Astafyeva, E., Rolland, L., and Sladen, A. (2014). Strike-slip earthquakes can also be detected in the ionosphere. *Earth and Planetary Science Letters*, 405(0):180 – 193.
- [Astafyeva et al. (2013)] Astafyeva, E., Shalimov, S., Olshanskaya, E., and Lognonné, P. (2013). Ionospheric response to earthquakes of different magnitudes: Larger quakes perturb the ionosphere stronger and longer. *GRL*, 40:1675–1681.
- [Berngardt et al. (2015)] Berngardt, O., Kotovich, G. V., Mikhailov, S. Y., and Podlesnyi, A. V. (2015). Dynamics of vertical ionospheric inhomogeneities over Irkutsk during 06:00-06:20ut 11/03/2011 caused by Tohoku earthquake. *Journal of Atmospheric and Solar-Terrestrial Physics*, 132:106-115.
- [Blanc (1985)] Blanc, E. (1985). Observations in the upper atmosphere of infrasonic waves from natural or artificial sources - A summary *Annales Geophysicae*, 3:673–687.
- [Calais and Minster (1995)] Calais, E. and Minster, J. B. (1995). GPS detection of ionospheric perturbations following the January 17, 1994, Northridge earthquake. *Geophysical Research Letters*, 22(9):1045–1048.
- [Chum et al. (2012)] Chum, J., Hruška, F., Zedník, J., and Laštovička, J. (2012). Ionospheric disturbances (infrasound waves) over the Czech

- Republic excited by the 2011 Tohoku earthquake. *Journal of Geophysical Research: Space Physics*, 117(A8):A08319.
- [Chum et al. (2016)] Chum, J., Liu, J.-Y., Laštovička, J., Fišer, J., Mošna, Z., Baše, J., and Sun, Y.-Y. (2016). Ionospheric signatures of the April 25, 2015 Nepal earthquake and the relative role of compression and advection for doppler sounding of infrasound in the ionosphere. *Earth, Planets and Space*, 68(1):1–12.
- [Haldoupis (2012)] Haldoupis, C. (2012). Midlatitude Sporadic E. A Typical Paradigm of Atmosphere-Ionosphere Coupling. *Space Science Reviews*, 168:441–461.
- [Haldoupis et al. (2006)] Haldoupis, C., Meek, C., Christakis, N., Pancheva, D., and Bourdillon, A. (2006). Ionogram height time intensity observations of descending sporadic E layers at mid-latitude. *Journal of Atmospheric and Solar-Terrestrial Physics*, 68:539–557.
- [Harris et al. (2012)] Harris, T. J., Cervera, M. A., Meehan, D. H. (2012), SpICE: A program to study small-scale disturbances in the ionosphere, *J. Geophys. Res.* 117:A06321
- [Harris et al. (2016)] Harris, T. J., Quinn, A. D., and Pederick, L. H. (2016). The DST group ionospheric sounder replacement for JORN. *Radio Science*, 51:563–572.
- [Jin et al. (2014)] Jin, S., Jin, R., and Li, J. H. (2014). Pattern and evolution of seismo-ionospheric disturbances following the 2011 Tohoku earthquakes from GPS observations. *Journal of Geophysical Research: Space Physics*, 119(9):7914–7927. 2014JA019825.
- [Jin et al. (2015)] Jin, S., Occhipinti, G., and Jin, R. (2015). {GNSS} ionospheric seismology: Recent observation evidences and characteristics. *Earth-Science Reviews*, 147(0):54 – 64.
- [Kakinami et al. (2013)] Kakinami, Y., Kamogawa, M., Watanabe, S., Odaka, M., Mogi, T., Liu, J. Y., Sun, Y. Y., and Yamada, T. (2013). Ionospheric ripples excited by superimposed wave fronts associated with Rayleigh waves in the thermosphere. *Journal of Geophysical Research (Space Physics)*, 118:905–911.
- [Kherani et al. (2012)] Kherani, E., Lognonné, P., Hebert, H., Rolland, L., Astafyeva, E., Occhipinti, G., Coisson, P., Walwer, D., and De Paula, E. (2012). Modelling of the total electronic content and

- magnetic field anomalies generated by the 2011 Tohoku-Oki tsunami and associated acoustic-gravity waves. *Geophysical Journal International*, 191(3):1049–1066.
- [Kherani et al. (2016)] Kherani, E., Rolland, L., Lognonné, P., Sladen, A., Klausner, V., and De Paula, E. (2016). Traveling ionospheric disturbances propagating ahead of the Tohoku-Oki tsunami: a case study. *Geophysical Journal International*, 204(2):1148–1158.
- [Kiryushkin et al. (2011)] Kiryushkin, V. V., Afraimovich, E., and Astafyeva, E. (2011). Evolution of seismo-ionospheric disturbances according to the data of dense network of GPS stations. *Cosmic Research*, 49:227–239.
- [Kozlovsky et al. (2013)] Kozlovsky, A., Turunen, T., Ulich, T. (2013), Rapid-run ionosonde observations of traveling ionospheric disturbances in the auroral ionosphere *J. Geophys. Res. Space Physics* 118, 5265–5276
- [Kurkin et al. (2014)] Kurkin, V.I. , Laryunin, O.A., Podlesny, A.V., Pezhemskaya, M.D., Chistyakova, L.V. Studying Morphological Characteristics of Traveling Ionospheric Disturbances with the Use of Near-Vertical Ionospheric Sounding Data *Atmospheric and Oceanic Optics*, 2014, Vol. 27, No. 4, pp. 303309.
- [Kuznetsov et al. (1999)] Kuznetsov, V. V., Plotkin, V. V., and Khomutov, S. Y. (1999). Acoustic, electromagnetic and ionospheric disturbances during the vibroseismic sounding. *Geophysical Research Letters*, 26(13):2017–2020.
- [Laštovička (2006)] Laštovička, J. (2006). Forcing of the ionosphere by waves from below. *Journal of Atmospheric and Solar-Terrestrial Physics*, 68(35):479 – 497.
- [Laštovička et al. (2010)] Laštovička, J., Baše, J., Hruška, F., Chum, J., Šindelářová, T., Horálek, J., Zedník, J., and Krasnov, V. (2010). Simultaneous infrasonic, seismic, magnetic and ionospheric observations in an earthquake epicentre. *Journal of Atmospheric and Solar-Terrestrial Physics*, 72:1231–1240.
- [Liu et al. (2011)] Liu, J.-Y., Chen, C.-H., Lin, C.-H., Tsai, H.-F., Chen, C.-H., and Kamogawa, M. (2011). Ionospheric disturbances triggered by the 11 March 2011 M9.0 Tohoku earthquake. *Journal of Geophysical Research: Space Physics*, 116(A6):A06319.

- [Liu et al. (2013)] Liu, J. Y., Chen, C. Y., and Sun, Y. Y. (2013). Wavy Structures in Vertical Electron Density Profile of the Ionosphere Triggered by the 2011 M9.0 Tohoku Earthquake. In *EGU General Assembly Conference Abstracts*, volume 15 of *EGU General Assembly Conference Abstracts*, 6097.
- [Liu et al. (2016)] Liu, J. Y. and Chen, C. H. and Sun, Y. Y. and Tsai, H. F. and Yen, H. Y. and Chum, J. and Laštovička, J. and Yang, Q. S. and Chen, W. S. and Wen, S. (2016). The vertical propagation of disturbances triggered by seismic waves of the 11 March 2011 M9.0 Tohoku earthquake over Taiwan *Geophysical Research Letters* 43(4), 1759–1765
- [Lognonné et al. (1998)] Lognonné, P., Clevede, E., and Kanamori, H. (1998). Computation of seismograms and atmospheric oscillations by normal-mode summation for a spherical Earth model with realistic atmosphere. *Geophysical Journal International*, 135:388–406.
- [Maruyama and Shinagawa (2013)] Maruyama, T. and Shinagawa, H. (2013). Vertically propagating acoustic waves launched by seismic waves visualized in ionograms. In *EGU General Assembly Conference Abstracts*, volume 15 of *EGU General Assembly Conference Abstracts*, 6472.
- [Maruyama and Shinagawa (2014)] Maruyama, T. and Shinagawa, H. (2014). Infrasonic sounds excited by seismic waves of the 2011 Tohoku-Oki earthquake as visualized in ionograms. *Journal of Geophysical Research: Space Physics*, 119(5):4094–4108.
- [Maruyama et al. (2011)] Maruyama, T., Tsugawa, T., Kato, H., Saito, A., Otsuka, Y., and Nishioka, M. (2011). Ionospheric multiple stratifications and irregularities induced by the 2011 off the pacific coast of Tohoku earthquake. *Earth, Planets, and Space*, 63:869–873.
- [Maruyama et al. (2016a)] Maruyama, T., Yusupov, K., and Akchurin, A. (2016a). Interpretation of deformed ionograms induced by vertical ground motion of seismic Rayleigh waves and infrasound in the thermosphere. *Annales Geophysicae*, 34(2):271–278.
- [Maruyama et al. (2016b)] Maruyama, T., Yusupov, K., and Akchurin, A. (2016b). Ionosonde tracking of infrasound wavefronts in the thermosphere launched by seismic waves after the 2010 M8.8 Chile earthquake. *Journal of Geophysical Research: Space Physics*, 121(3):2683–2692.

- [Matsumura et al. (2011)] Matsumura, M., Saito, A., Iyemori, T., Shinagawa, H., Tsugawa, T., Otsuka, Y., Nishioka, M., and Chen, C. H. (2011). Numerical simulations of atmospheric waves excited by the 2011 off the Pacific coast of Tohoku Earthquake. *Earth, Planets, and Space*, 63:885–889.
- [Munro and Heisler (1956)] Munro, G.H., Heisler, L.H. (1956). Cusp Type Anomalies in Variable Frequency Ionospheric Records *Australian Journal of Physics*, 9(3): 343–358
- [Nishitani et al. (2011)] Nishitani, N., Ogawa, T., Otsuka, Y., Hosokawa, K., and Hori, T. (2011). Propagation of large amplitude ionospheric disturbances with velocity dispersion observed by the SuperDARN Hokkaido radar after the 2011 off the Pacific coast of Tohoku Earthquake. *Earth, Planets, and Space*, 63:891–896.
- [Occhipinti et al. (2008)] Occhipinti, G., Kherani, E., and Lognonné, P. (2008). Geomagnetic dependence of ionospheric disturbances induced by tsunamigenic internal gravity waves. *Geophysical Journal International*, 173:753–765.
- [Perevalova et al. (2014)] Perevalova, N., Sankov, V., Astafyeva, E., and Zhupityaeva, A. (2014). Threshold magnitude for ionospheric {TEC} response to earthquakes. *Journal of Atmospheric and Solar-Terrestrial Physics*, 108:77 – 90.
- [Perevalova et al. (2015)] Perevalova, N., Shestakov, N., Voeykov, S. V., Takahashi, H., and Guojie, M. (2015). Ionospheric disturbances in the vicinity of the Chelyabinsk meteoroid explosive disruption as inferred from dense GPS observations. *Geophysical Research Letters, Geophys. Res. Lett.*, 42(16):6535–6543.
- [Podlesnyi et al (2011)] Podlesny, A.V., Kurkin, V.I., Medvedev, A.V., Ratovsky, K.G. (2011) Vertical ionosphere sounding using continuous signals with linear frequency modulation *Proceedings of XXIX General Assembly and Scientific Symposium. Istanbul, Turkey, August 13-20, 2011* P. HP1-2. (<http://www.ursi.org/proceedings/procGA11/ursi/HP1-2.pdf>)
- [Podlesnyi et al (2013)] Podlesnyi, A.V., Brynko, I.G., Kurkin, V.I., Berezovsky, V.A., Kiselyov, A.M., Petuchov, E.V., Multifunctional chirp ionosonde for monitoring the

- ionosphere (in russian) *Heliogeophysical Research*, 4, 24-31,
(<http://vestnik.geospace.ru/php/download.php?id=UPLF41dc6e89d6cba19d27b9039718718>)
- [Podlesnyi et al (2014a)] Podlesnyi, A.V., Lebedev, V.P., Ilyin, N.V., Khakhinov, V.V.(2014a), Implementation of method for constructing ionospheric radio channel transfer function from results of ionospheric sounding by frequency-modulated continuous wave(in russian) *Electromagnitnie volny i elektronnie sistemi (Electromagnetic waves and electronic systems)* 19(1):063–070
- [Podlesnyi et al (2014b)] Podlesnyi, A.V., Kurkin, V.I., Laryunin, O.A., Pezhemskaya, M.D., Chistyakova, L.V. (2014b) Studying travelling ionospheric disturbances from near - vertical ionosphere sounding with high temporal resolution Proceedings of XXX URSI General Assembly and Scientific Symposium. Beijing, China. August 16-23, 2014, GP2.27 ([http : //www.ursi.org/proceedings/procGA14/papers/ursi_paper2518.pdf](http://www.ursi.org/proceedings/procGA14/papers/ursi_paper2518.pdf)).
- [Pokhotelov (1995)] Pokhotelov, O.A., Parrot, M., Fedorov, E.N., Pilipenko, V.A., Surkov, V.V., Gladychiev, V. A. (1995). Response of the ionosphere to natural and man-made acoustic sources *Annales Geophysicae*, 13(11):1197–1210
- [Ponyatov et al. (1999)] Ponyatov, A. A., Uryadov, V. P., Ivanov, V. A., Ivanov, D. V., Chernov, A. G., Shumaev, V. V., Cherkashin, Yu. N.(1999).Oblique chirp sounding of the modified ionosphere. Experiment and simulation *Radiophysics and Quantum Electronics*,42(4):269–277
- [Reinisch et al (2009)] Reinisch, B. W., Galkin, I.A., Khmyrov, G. M., Kozlov, A. V., Bibl, K., Lisysyan, I. A., Cheney, G. P., Huang, X., Kitrosser, D. F., Paznukhov, V. V., Luo, Y., Jones, W., Stelmash, S., Hamel, R., Grochmal, J. (2009) New Digisonde for research and monitoring applications, *Radio Science* 44(1):RS0A24.
- [Rolland (2011)] Rolland, L. (2011). Three-dimensional numerical modeling of tsunami-related internal gravity waves in the Hawaiian atmosphere. *Earth, Planets, and Space*, 63:847–851.
- [Shinagawa et al. (2007)] Shinagawa, H., Iyemori, T., Saito, S., and Maruyama, T. (2007). A numerical simulation of ionospheric and atmospheric variations associated with the Sumatra earthquake on December 26, 2004. *Earth, Planets and Space*, 59(9):1015–1026.

- [Shinagawa et al. (2013)] Shinagawa, H., Tsugawa, T., Matsumura, M., Iyemori, T., Saito, A., Maruyama, T., Jin, H., Nishioka, M., and Otsuka, Y. (2013). Two-dimensional simulation of ionospheric variations in the vicinity of the epicenter of the Tohoku-Oki earthquake on 11 March 2011. *Geophysical Research Letters*, 40(19):5009–5013.
- [Smaryshev (1973)] Smaryshev, M.D. (1973). Directivity of hydroacoustical antennas(in russian) *Sudostroenie, Leningrad*.
- [Steblov et al. (2014)] Steblov, G. M., Ekstrm, G., Kogan, M. G., Freymueller, J. T., Titkov, N. N., Vasilenko, N. F., Nettles, M., Gabsatarov, Y. V., Prytkov, A. S., Frolov, D. I., and Kondratyev, M. N. (2014). First geodetic observations of a deep earthquake: The 2013 Sea of Okhotsk Mw 8.3, 611 km-deep, event. *Geophysical Research Letters*, 41(11):3826–3832..
- [Tang et al. (2015)] Tang, L., Zhang, X., and Li, Z. (2015). Observation of ionospheric disturbances induced by the 2011 Tohoku tsunami using far-field GPS data in Hawaii. *Earth, Planets and Space*, 67:88.
- [Ye et al. (2013)] Ye, L., Lay, T., Kanamori, H., and Koper, K. D. (2013). Energy release of the 2013 Mw 8.3 Sea of Okhotsk earthquake and deep slab stress heterogeneity. *Science*, 341(6152):1380–1384.
- [Zhan et al. (2014)] Zhan, Z., Kanamori, H., Tsai, V. C., Helmberger, D. V., and Wei, S. (2014). Rupture complexity of the 1994 Bolivia and 2013 Sea of Okhotsk deep earthquakes. *Earth and Planetary Science Letters*, 385:89–96.
- [Zharebtsov et al. (2012)] Zharebtsov, G.A. (2012) Seismoionospheric and seismoelectromagnetic processes in the Baikal rift zone(in russian), (edit. Zharebtsov G.A.) *Novosibirsk. Publishing house of the Siberian Branch of the Russian Academy of Sciences*.
- [IRIS/IDA Seismic Network ()] IRIS/IDA Seismic Network, <http://dx.doi.org/doi:10.7914/SN/II>
- [Global Seismograph Network ()] Global Seismograph Network (GSN - IRIS/USGS) (GSN), <http://dx.doi.org/doi:10.7914/SN/IU>
- [Synthetic Seismograms Network ()] Synthetic Seismograms Network, <http://www.fdsn.org/networks/detail/SY/>
- [POLAN Program ()] POLAN Program, <http://www.ursi.org/files/CommissionWebsites/INAG/>